10098 *Biochemistry* **2010,** *49,* 10098–10106
DOI: 10.1021/bi101198n

BIOCHEMISTRY
including biophysical chemistry & molecular biology
Article

Water Oxidation by Photosystem II: H_2O-D_2O Exchange and the Influence of pH Support Formation of an Intermediate by Removal of a Proton before Dioxygen Creation[†]

László Gerencsér* and Holger Dau*

Freie Universität Berlin, FB Physik, Arnimallee 14, D-14195 Berlin, Germany

Received July 29, 2010; Revised Manuscript Received October 8, 2010

ABSTRACT: Understanding the chemistry of photosynthetic water oxidation requires deeper insight into the interrelation between electron transfer (ET) and proton relocations. In photosystem II membrane particles, the redox transitions of the water-oxidizing Mn complex were initiated by nanosecond laser flashes and monitored by absorption spectroscopy at 360 nm (A_{360}). In the oxygen evolution transition ($S_3 + h\nu \rightarrow S_0 + O_2$), an exponential decrease in A_{360} (τ_{O_2} = 1.6 ms) can be assigned to Mn reduction and O_2 formation. The corresponding rate-determining step is the ET from the Mn complex to a tyrosine radical (Y_Z^{ox}). We find that this A_{360} decrease is preceded by a lag phase with a duration of 170 ± 40 μs (τ_{lag} at pH 6.2), indicating formation of an intermediate before ET and O−O bond formation and corroborating results obtained by time-resolved X-ray spectroscopy. Whereas τ_{O_2} exhibits a minor kinetic isotope effect and negligible pH dependence, formation of the intermediate is slowed significantly both in D_2O (τ_{lag} increase of ∼140% in D_2O) and at low pH (τ_{lag} of 30 ± 20 μs at pH 7.0 vs τ_{lag} of 470 ± 80 μs at pH 5.5). These findings support the fact that in the oxygen evolution transition an intermediate is created by deprotonation and removal of a proton from the Mn complex, after Y_Z^{ox} formation but before the onset of electron transfer and O−O bond formation.

Photosynthetic oxygen evolution in higher plants and cyanobacteria is catalyzed by the oxygen-evolving complex (OEC), a Mn_4Ca complex bound to the proteins of photosystem II (PSII) (*1*−*3*). The crystal structure of PS II provides insights into the location and approximate arrangement of the four Mn and single Ca ions (*4*−*6*), which together with bridging and terminal ligands form the entity here denoted the "Mn complex". The high rate and efficiency of water oxidation by the Mn complex of PSII (*7*, *8*) presently are unmatched by any synthetic catalyst (see ref *9*). Elucidating the reason(s) for the superior performance of the biological catalyst represents an important challenge. One key aspect is the "smart" coupling of electron transfer (ET)[1] and accumulation of oxidizing equivalents with proton relocations (*1*, *8*−*14*).

Excitation of PSII by a quantum of light initiates a sequence of ET reactions. After formation of the primary radical pair, the cation radical is stabilized on a Chl molecule, which is denoted as P_{680} (*15*−*17*), and an electron is transferred to a bound quinone (Q_A). Subsequently, P_{680}^+ is reduced, largely within less than 1 μs, by a redox-active tyrosine denoted Y_Z (Tyr_{161} of the D1 protein of PSII). Initially, the difference in free energy (ΔG_0) for the ET from Y_Z to P_{680}^+ is small; a quasi-equilibrium prevails with an easily detected population of the P_{680}^+ state (*18*, *19*). This P_{680}^+ population decays on a clearly slower time scale (in the microsecond domain, up to 100 μs or even slower), likely reflecting "relaxation" of the Y_Z^{ox} environment by proton rearrangements (*18*, *19*). The $Y_Z \rightarrow P_{680}^+$ ET is followed by the reduction of Y_Z^{ox} and oxidation of the Mn complex with ET time constants of 30−1500 μs (*20*−*23*). The successive absorption of four light quanta by PS II eventually results in the accumulation of four oxidizing equivalents in the OEC, which is the prerequisite for the subsequent oxidation of the two "substrate" water molecules and the coupled O_2 release (Figure 1A). The accumulation of oxidizing equivalents is discussed in terms of the S-state cycle model outlined below.

Kok and co-workers developed a reaction cycle model involving the light-driven formation of five S_i states (i = 0, ..., 4) of the OEC, where the subscript indicates the number of accumulated oxidizing equivalents (*24*) (Figure 1A). After formation of the S_4 state, dioxygen is formed and the catalyst is set back to the S_0 state (*24*, *25*). Later accumulation of oxidizing equivalents was found to be associated with oxidation of Mn ions likely involving the following oxidation-state combinations: S_0, $Mn_3^{III}Mn^{IV}$; S_1, $Mn_2^{III}Mn_2^{IV}$; S_2, $Mn^{III}Mn_3^{IV}$; S_3, Mn_4^{IV} (*11*, *26*). Also other

[†]This work was supported by the European Union (7th framework program, SOLAR-H2 consortium), the Federal Ministry of Education and Research of Germany (BMBF, H_2 Design Cell, 03SF0355D), and the Berlin cluster of excellence on Unifying Concept in Catalysis (UniCat). L.G. gratefully acknowledges a postdoctoral fellowship from the Alexander-von-Humboldt (AvH) foundation.

*To whom correspondence should be addressed: Freie Universität Berlin, Arnimallee 14, D-14195 Berlin, Germany. Telephone: +49-30-8385-3581. Fax: +49-30-8385-6299. E-mail: laszlo.gerencser@fu-berlin.de (L.G.) or holger.dau@fu-berlin.de (H.D.).

[1]Abbreviations: Chl, chlorophyll; D1, protein subunit of PSII encoded by the *psbA* gene; E_m, redox midpoint potential; EPR, electron paramagnetic resonance spectroscopy; ET, electron transfer; IR, infrared; KIE, kinetic isotope effect; LED, light-emitting diode; MES, 2-(*N*-morpholino)ethanesulfonic acid; MOPS, 3-(*N*-morpholino)-propanesulfonic acid; P_{680}, chlorophyll radical in PSII, oxidant of Y_Z; Q_A, primary quinone acceptor in PSII; Q_B, secondary quinone acceptor in PSII; UV, ultraviolet; Y_Z, Tyr_{161} of the D1 protein.

 Published on Web 10/21/2010

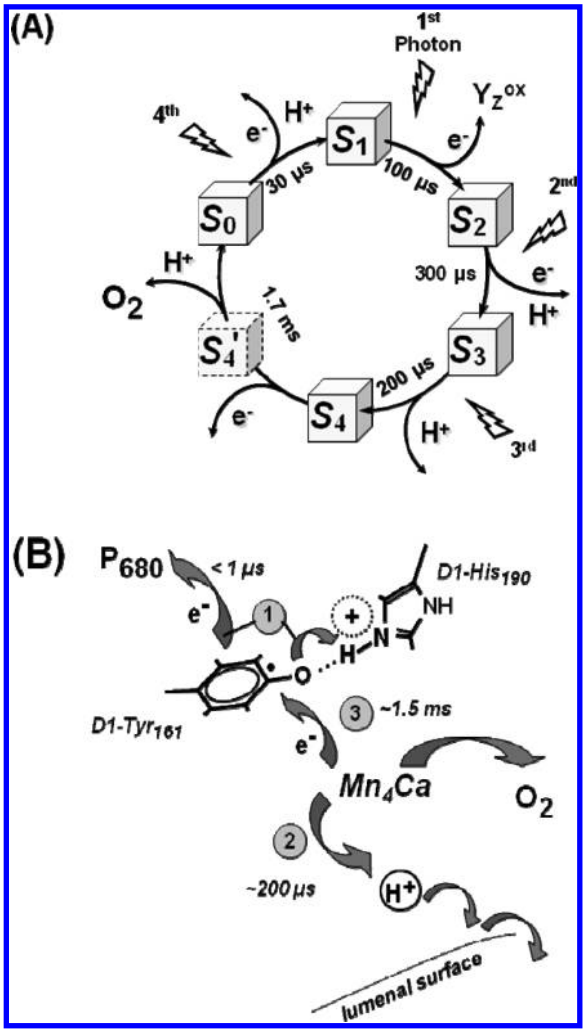

FIGURE 1: Kok's classical S-state cycle model extended by one intermediate state that is formed by deprotonation (*23*). (A) The S_4 state is formed by deprotonation of the Mn_4Ca complex or its ligand environment. In this state, a total of four oxidizing equivalents (OE) has been accumulated by the Mn complex (three OE) and the Tyr_{161} of the D1 protein (Y_Z^{ox}, one OE). In the subsequently formed S_4' state, four OE are assumed to be located on the Mn complex itself, before the onset of dioxygen formation. Formation of this S_4' state has not been detected experimentally; it may resemble a transition state. Recently (*1*), an extended S-state cycle model in which states S_3, S_4, and S_4' have been denoted S_3^+, S_3^n, and S_4^+, respectively, has been described. The proton release indicated in panel A is in agreement with the commonly assumed stoichiometry for the removal of "intrinsic" or "chemical" protons from the catalytic site (*12*, *31*−*34*); the indicated electron removal always proceeds via the transfer of an electron to Y_Z^{ox} but is indicated in panel A for only the first flash. (B) Proposed spatiotemporal sequence of events in the $S_3 + h\nu \rightarrow S_0 + O_2$ transition: (1) transfer of an electron from Y_Z to P_{680}^+ and a shift of a proton within the hydrogen bond between Y_Z and His_{190}, (2) deprotonation of the Mn_4Ca complex and relocation of a proton to the lumenal bulk phase, and (3) transfer of an electron from the Mn_4Ca complex to Y_Z^{ox} and O_2 formation. All indicated time constants refer to typical experimental values determined at pH 6.2 (panels A and B modified from ref *23*).

oxidation-state assignments have been discussed (*27*−*30*). The accumulation of four oxidizing equivalents does not correspond to accumulation of four charges because the S-state transitions of the OEC are accompanied by proton release, either by chemical liberation from the Mn complex or by electrostatically induced p*K* shifts of peripheral residues (*12*, *31*−*34*). The spatiotemporal orchestration of ET and proton relocations remains insufficiently understood. Recent results suggest that "smart" coupling among ET, short-range proton shifts, and long-range proton relocations may be essential for efficient water oxidation, as discussed elsewhere (*1*, *7*, *9*, *35*).

In this investigation, we focus on formation of an intermediate state in the oxygen evolution transition induced dominantly by the third saturating flash of visible light applied to dark-adapted PSII; that is, we investigate a reaction intermediate in the overall $Y_Z^{ox}S_3 \rightarrow Y_ZS_0 + O_2$ transition. For this oxygen evolution transition, time-resolved X-ray absorption spectroscopy has provided clear evidence that an intermediate state is formed within ~200 μs after Y_Z^{ox} formation but before ET (from the Mn complex to Y_Z^{ox}) and dioxygen formation, as described in ref *23* and detailed elsewhere (*25*). In ref *23*, formation of the new intermediate in the reaction cycle has been assigned to deprotonation and relocation of a proton from the Mn complex to the aqueous bulk phase. This assignment resulted partly from an analysis of delayed fluorescence data that suggested an entropy-driven process with a pH-dependent driving force, as expected for the release of a proton to the aqueous bulk (*23*, *36*, *37*). A second line of evidence came from an elegant study presented in 1994 by Rappaport and co-workers (*21*). They used a special pump−probe approach for near-UV measurements on electron transfer and electrochromism and detected in the oxygen evolution transition, a fast electrochromic decay accompanied by a lag in the ET kinetics, both with half-times of ~30 μs. This 30 μs phase was interpreted, in 1994, as a reflection of the electrostatically triggered expulsion of one proton from the catalytic center by the positive charge on Y_Z^{ox} (*21*). Visual inspection of the data of Rappaport and co-workers (*21*) suggests that their 30 μs lag phase could be in agreement with the 200 μs lag in the ET kinetics found in the time-resolved X-ray experiment (*23*), as also stated by Rappaport and Diner (*8*). Therefore, we consider it likely that the results presented in refs *21* and *23* relate to the same processes. In conclusion, time-resolved detection of electrochromism (*21*) and delayed Chl fluorescence (*23*) have provided circumstantial evidence of the assignment of the process of intermediate formation to deprotonation of the catalytic site and proton release (*12*, *38*). Our study aims at providing further experimental support by investigation of the D_2O-H_2O exchange effect and influence of pH on the rate of intermediate formation.

In the X-ray absorption experiments mentioned above (*23*, *25*), the oxidation-state changes of the Mn ions in PSII were monitored for excitation at different X-ray energies in the region of the K-edge of manganese (*39*). A delay or lag phase (τ_{lag}, duration of ~200 μs) visible in the X-ray transients before onset of the Mn reduction and O_2 release (τ_{O_2} of ~1.6 ms) suggested the formation of a reaction intermediate (*23*). In several earlier studies, oxidation-state changes of the Mn complex were monitored by recording absorption change in the (near) UV region (*20*−*22*, *40*, *41*). In only two studies was it concluded that a lag phase indicative of intermediate formation is present in the near-UV transients of the oxygen evolution transition (*21*, *41*). Recently, the existence of the lag phase in the X-ray and UV transients has been questioned (*42*).

In this work, near-UV absorption transients were measured employing a home-built kinetic spectrophotometer for collection of data on PSII membrane particles at a high signal-to-noise ratio. We show that formation of the precursor state in the oxygen evolution transition is indeed detectable in the near-UV transients. A pronounced pH dependence and sizable H−D kinetic isotope effect support the hypothesis that formation of the precursor state can be assigned to deprotonation and proton release.

MATERIALS AND METHODS

Sample Preparation and Characterization. PSII membrane particles (*43*) were prepared from spinach as described in ref *44*. The oxygen evolution activity under actinic continuous illumination was 1200−1400 μM O_2 (mg of Chl)$^{-1}$ h^{-1} at 28 °C in the presence of 0.3 mM 2,6-dichloro-*p*-benzoquinone (2,6-DCBQ) and 5 mM $K_3[Fe(CN)_6]$. For sample preparation, aliquots of PSII membranes were thawed, carefully homogenized to minimize light scattering in the UV measurements, and suspended at 15 μM Chl in buffer D [1 M glycine-betaine, 25 mM MES, 10 mM NaCl, 5 mM $CaCl_2$, and 5 mM $MgCl_2$ (pH 6.2)]. Measurements at pH < 5.5 or > 6.5 were taken in the presence of 25 mM sodium citrate and 25 mM MOPS, respectively. The H_2O content of the sample solubilized in D_2O was reduced below 1% when the sample was washed twice in buffer D prepared with D_2O. Time-resolved prompt Chl fluorescence measurements were taken as described in ref *37*.

Near-UV Absorption Changes. Absorption changes of the PSII particles were measured at 360 nm (A_{360}) using a home-built kinetic spectrophotometer. The white light of a 200 W halogen lamp (Heraeus, CT 200T01) passed a double-grating monochromator (from Shimadzu RF-502, 7.5 nm bandwidth) and was focused onto the surface of the photocathode of the detecting photomultiplier (PM, Electron tubes, 9734B). The measuring light illuminated the sample for 20 ms before and 20 ms after each exciting laser flash as controlled by a photoshutter (Uniblitz Vincent Associates, VS25S2T1). During this light period (40 ms), less than 5% of the PSII centers were excited by the measuring light. The operation of the shutter was accompanied by a sudden, enormous change in the light intensity at the surface of the photocathode, which caused a light hysteresis effect of the PM. To avoid this effect, the cathode surface was illuminated by a LED replacing the measuring light when the shutter was closed. The PM was protected against scattered laser light and fluorescence of the sample by interference (Asahi spectra, ASA ZBPA 360) and bandpass (Schott, BG3, 3 mm) filters. The sample was excited perpendicular to the measuring beam by a frequency-doubled, Q-switched Nd:YAG laser (Quantel Brilliant B, 532 nm, 5 ns full width at half-maximum). The energy density of the laser flash was attenuated by a Glan Taylor prism (Topag Lasertechnik) to 4.5 mJ/cm^2 as measured by a power meter (Ophir PD300), which was sufficient to fully saturate the PSII centers. The PM signal was amplified by a differential low-noise preamplifier (Stanford Research Systems, SR560; selected bandwidth of 1 MHz), and the signal was digitized with an A/D converter (Adlink PCI-9812, sampling frequency of 4 MHz). The data used for curve fitting (in Origin version 7.5, OriginLab) and display in this work were obtained by averaging 10 neighboring points, which corresponds to a time interval of 2.5 μs; exclusively for the $S_3 + h\nu \rightarrow S_0 + O_2$ transition, 40 points were averaged (10 μs). Uncertainty ranges of fit parameters represent the one-σ range, as determined by the respective routines of Origin version 7.5.

The signal-to-noise ratio was increased by averaging the transients of 500 PSII samples, measured effectively using an automatic sample-change system. Each sample was pumped from a light-protected reservoir (at 4 °C) into the flow-through cuvette (Hellma, 131-QS) by a peristaltic pump (Cole Palmer 77521-47), excited by a series of 16 laser flashes, and removed. Binary oscillations in the UV transients relating to the two-electron chemistry of the secondary quinone (Q_B) at the reducing site of PSII were suppressed by addition of electron acceptors {100 μM 2,6-DCBQ and 0.5 mM $K_3[Fe(CN)_6]$}. The flash spacing was 1.4 s to allow for the complete reoxidation of Q_B^- between flashes (*45*). There remained a small, slow, and flash number-independent acceptor side contribution ($\tau \sim 100-200$ ms) which was subtracted, as shown in Figure S1 of the Supporting Information. All measurements were taken at 23 °C.

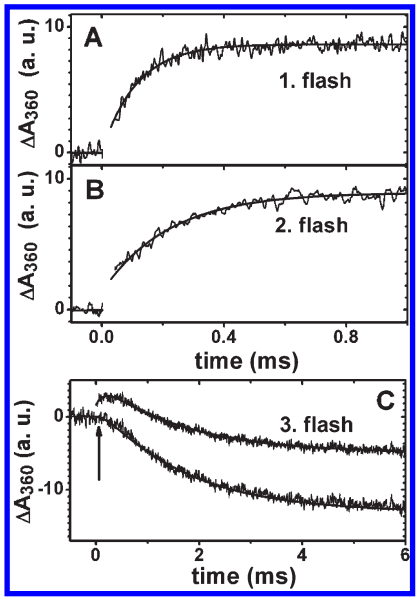

FIGURE 2: Transfer of an electron from the Mn complex to Y_Z^{ox} monitored by detection of absorption changes at 360 nm (pH 6.2). The $S_1 \rightarrow S_2$ transition is induced by excitation with the first nanosecond laser flash (A); the second flash induces the $S_2 \rightarrow S_3$ transition in the clear majority of photosystems (B). The third flash induces mostly the $S_3 \rightarrow S_0 + O_2$ transition (top curve in panel C). The bottom curve in panel C was obtained by correction (deconvolution) for the rapid rise resulting from Q_A^- formation, for miss events on the first two flashes, and for the influence of PSII defective in the acceptor side ET from Q_A to Q_B.

RESULTS

Time Course of Flash-Induced Absorption Changes. The S-state transitions of the OEC were monitored at 360 nm, where the $Q_A^-Q_B \rightarrow Q_AQ_B^-$ ET and the $Y_Z \rightarrow Y_Z^{ox} \rightarrow Y_Z$ redox changes do not contribute [isosbestic point (*46*)]. The first flash excitation of the dark-adapted PSII sample (being predominantly in the S_1 state) induced an absorption increase due to the formation of Q_A^- [rise time of ~300 ps (*47*)] and a well-resolved slower rise assigned to Mn oxidation in the $Y_Z^{ox}S_1 \rightarrow Y_ZS_2$ transition (Figure 2A). (In the following, for the sake of simplicity, the $Y_Z^{ox}S_i \rightarrow Y_ZS_{i+1}$ transition is denoted as $S_i \rightarrow S_{i+1}$.) Curve fitting of the slow-rise phase, assuming an exponential behavior, yielded a time constant of 100 ± 5 μs, in good agreement with previous results (*20*−*23*, *48*).

The second-flash excitation initiated a similar absorption change. The slow rise can largely be assigned to Mn oxidation in the $S_2 \rightarrow S_3$ transition and is slower than in the $S_1 \rightarrow S_2$ transition (Figure 2B). In a minor fraction of PSII centers, the $S_1 \rightarrow S_2$ transition took place due to so-called miss events and due to a subpopulation of PSII denoted as non-Q_B units (*45*, *49*). The miss events are described by a miss parameter [α = 7−15% (*24*)] and results from a quantum efficiency (η) of the light-induced S-state transitions of less than 100% ($\eta = 1 - \alpha$) (*50*). In non-Q_B units, the forward transfer of an electron from Q_A^- to Q_B is

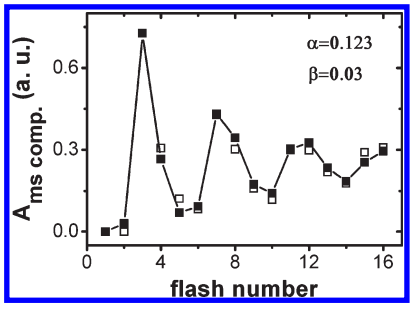

FIGURE 3: Period-of-four oscillation of the amplitude of the millisecond decrease in the A_{360} transients collected at pH 6.2 (□). The data were simulated on the basis of Kok's S-state cycle model (■). Curve fitting resulted in a value for the miss parameter (α) of 12.3%. A small fraction of PSII experiencing a double hit (β = 3%) increased the fit quality significantly, whereas a non-zero value of the S_0 population in dark-adapted samples did not result in any improvement.

blocked so that charge recombination ($S_2Q_A^- \rightarrow S_1Q_A$) takes place in some PSII. Considering the applied flash spacing (1.4 s) and the time constant of the charge recombination (4.8 s in refs *51* and *52*), 25% of the $S_2Q_A^-$ state was estimated to recombine to the S_1Q_A state.

The absorption transient induced by the third flash was more complex (Figure 2C, top curve). After the rapid absorption increase (rapid Q_A reduction), a small rising phase and a lag phase were observable, within the first 500 μs of the laser flash. The lag-phase behavior relates to the formation of a precursor state in the oxygen evolution transition, as discussed in the following. The rise or lag is partially attributable also to induction of lower S-state transitions in a fraction of PSII being in the S_2 state (due to miss events) or S_1 state (due to recombination in non-Q_B units) before excitation by the third flash. After the rise or lag phase, an absorption decrease is observed, reflecting Mn reduction in the O_2 evolution step.

Influence of Miss Events and Non-Q_B Units. Miss events and the existence of non-Q_B units cause desynchronization of the advancement in the S-state cycle. Because this desynchronization affects the lag-phase behavior visible in the measured third-flash transient significantly, a correction is approached. This correction procedure, also denoted as "deconvolution" (*45*, *47*, *53*), is rooted in Kok's S-state cycle model and involves determination of the parameters for miss events (α) and double hits (β) as well as estimates of the number of recombining non-Q_B units. For the determination of α, the absorption transients induced by the first 16 flashes were simulated by a sum of exponentials using an identical time constant (τ_{O_2} = 1.6 ms) for the millisecond phase that parallels dioxygen formation, in each of the 16 transients. Thereby the flash number (n) dependence of the amplitude of the millisecond phase, $A_{O_2}(n)$, was obtained. $A_{O_2}(n)$ was fitted on the basis of Kok's S-state model (Figure 3), resulting in values for α (12%) and β (3%). The small but non-zero value for β reflects apparent double hits caused by the actinic effect of measuring light in 3% of the PSII. The fraction of the non-Q_B units (q) was estimated on the basis of measurements of the prompt Chl fluorescence (data not shown). After the determination of α, β, and q, the measured transients were corrected accordingly, resulting in deconvoluted transients (see the Supporting Information for details).

After deconvolution, the simulation of the absorption transient of the $S_2 \rightarrow S_3$ transition yielded a time constant of 280 ± 15 μs, which is in agreement with most previous studies (*20*−*23*, *48*). In the absorption transient of the $Y_Z^{ox}S_3 \rightarrow Y_ZS_0 + O_2$ transition

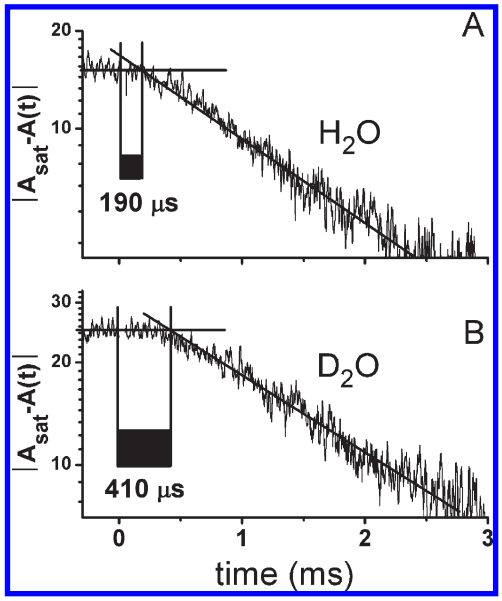

FIGURE 4: Semilogarithmic plot illustrating the delayed onset of Mn reduction (lag-phase behavior) in the $Y_Z^{ox}S_3 \rightarrow Y_Z^0S_0 + O_2$ transition. The difference between the A_{360} signal and the level reached at ~20 ms is plotted. The lag-phase durations indicated in the figure were estimated from the intersection of the baseline and a straight line describing the slow changes in A_{360}. The duration increased from ~190 to 410 μs via replacement of H_2O with D_2O, which corresponds to a sizable H−D kinetic isotope effect ($k_{H_2O}/k_{D_2O} \approx 2.2$).

induced by the third flash, the rise or lag behavior was modified strongly by the deconvolution procedure and a sigmoidal decrease became pertinent (Figure 2C, bottom curve; see also Figure 4). (For the sake of simplicity, in the following $Y_Z^{ox}S_3 \rightarrow Y_ZS_0 + O_2$ is abbreviated as $S_3 \rightarrow S_0 + O_2$.) Assuming a consecutive reaction, the deconvoluted $S_3 \rightarrow S_0 + O_2$ transient was simulated according to

$$A(t) = A_{max}\left[1 + \frac{k_{lag}\exp(-k_{O_2}t) - k_{O_2}\exp(-k_{lag}t)}{k_{O_2} - k_{lag}}\right] \quad (1)$$

Time constants of 170 ± 40 μs ($\tau_{lag} = 1/k_{lag}$, lag phase) and 1.6 ms ($\tau_{O_2} = 1/k_{O_2}$, ET paralleled by oxygen evolution) were obtained. Both figures agree well with those derived from X-ray absorption data [τ_{lag} = 200 μs, and τ_{O_2} = 1.6 ms (*23*)]; the oxygen evolution time constant (τ_{O_2}) is similar to values reported previously (*20*−*22*, *48*).

The strong influence of the deconvolution prompted us to assess how the duration of the lag phase is altered by variation of the critical parameters, i.e., the miss probability (α) and the fraction of non-Q_B units (q). These parameters were varied around the best-estimate value (α = 0.123, 15% of non-Q_B units), and the time constant of the lag phase was determined for each parameter set (Table S1 of the Supporting Information); we found that the lag-phase duration varied strongly (between 80 and 270 μs). However, even for extreme parameters, a lag-phase behavior could be observed. We conclude that the precision of the deconvolution is critical for the duration of the lag phase but does not call into question its existence. In the following, the α value is used for deconvolution that resulted from the best fit of the respective A_{O_2} pattern (see Figure 3, for pH 6.2 in H_2O).

H−*D Kinetic Isotope Effect on the Lag-Phase Duration.* For PSII dissolved in deuterated water (H_2O−D_2O exchange), the miss parameter was found to be increased significantly (by 4% to a value of 16.3% at pD 6.2), as observed previously (*41*). The lag-phase duration was significantly increased by replacement

Table 1: Time Constants (in microseconds) Determined by Curve Fitting of Deconvoluted A_{360} Transients

	pH 6.2	pD 6.2	τ_D/τ_H	pH 5.5	pH 7.0	$\tau_{5.5}/\tau_{7.0}$
τ_{ET} in $S_1 \rightarrow S_2$	100 ± 5	115 ± 5	1.15	100 ± 5	95 ± 5	1.05
τ_{ET} in $S_2 \rightarrow S_3$	280 ± 20	480 ± 20	1.7	300 ± 15	260 ± 15	1.15
τ_{lag} in $S_3 \rightarrow S_0 + O_2$	170 ± 40	405 ± 50	2.4	470 ± 80	30 ± 25	> 7
τ_{O_2} in $S_3 \rightarrow S_0 + O_2$	1670 ± 50	1950 ± 50	1.17	1820 ± 50	1770 ± 50	1.03

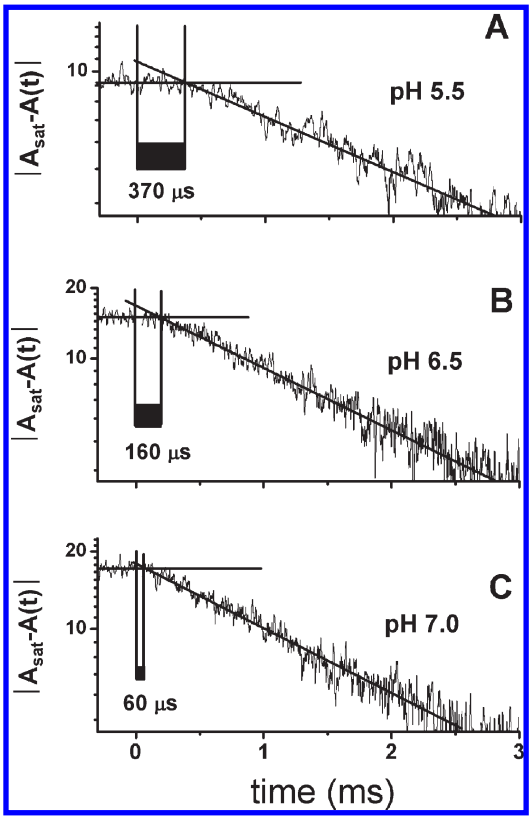

FIGURE 5: Duration of the lag phase at three pH values. For details, see the legend of Figure 4.

of H_2O with D_2O (Figure 4). Simulations based on a consecutive reaction scheme (eq 1) indicate an increase from 170 μs (H_2O) to 405 μs (D_2O) corresponding to deceleration by a factor of 2.38 [$= k_H/k_D$ (KIE)]. In contrast, the millisecond decay component exhibited a deceleration from 1.67 ms (H_2O) to 1.95 ms (D_2O), which corresponds to a KIE of only 1.17 (Table 1).

pH Dependence of the Lag-Phase Duration. An increased miss probability results from lowering of the pH (Figure S2 of the Supporting Information), as described previously (*50*, *54*, *55*). The increase is not distributed equally on the four S-state transitions but can be attributed exclusively to the $S_3 \rightarrow S_0 + O_2$ transition for pH > 5 (*56*, *57*). Therefore, the deconvolution was conducted assuming that for all other S-state transitions, the miss probability is independent of pH ($\alpha = 0.123$).

We observe a pronounced pH dependence of the lag-phase duration (Figures 5 and τ_{lag} in Figure 6). In clear contrast, the rate of ET and O_2 formation is essentially pH-independent (τ_{O_2} in Figure 6), in line with results of previous investigations (*21*, *41*, *58*).

The effect of pH and H−D exchange on the reaction kinetics (time constants) of the $S_3 \rightarrow S_0 + O_2$ transition are summarized in Table 1, including selected kinetic parameters determined for the $S_1 \rightarrow S_2$ and $S_2 \rightarrow S_3$ transitions. The relation to proton

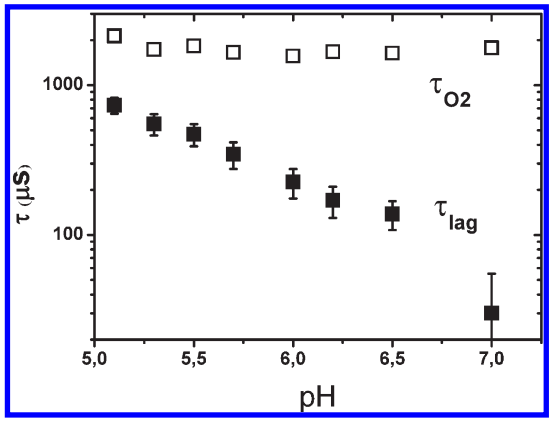

FIGURE 6: pH dependence of τ_{lag} (■) and τ_{O_2} (□). The deconvoluted A_{360} transients of the $S_3 \rightarrow S_0 + O_2$ transition were simulated assuming a consecutive reaction scheme (eq 1). The time constants and error ranges are shown using a logarithmically scaled *y*-axis.

transfer of the reaction intermediate formed in the course of the $S_3 \rightarrow S_0 + O_2$ transition is suggested by the sizable H−D isotope effect and strong pH dependence of the lag-phase duration. The weaker but still relatively strong kinetic isotope effect (KIE) of the $S_2 \rightarrow S_3$ transition also suggests a relation to proton transfer, as concluded previously (*22*, *41*, *59*). However, coupling of the $S_1 \rightarrow S_2$ transition and the oxygen evolution transition to proton transfer is not suggested by the kinetic data summarized in Table 1. We note that the $S_0 \rightarrow S_1$ transition has not been resolved in our experiments; previously negligible H−D exchange and pH effects have been reported for this transition (*41*).

DISCUSSION

Tracking Mn Oxidation States: X-ray versus Near-UV Spectroscopy. By X-ray absorption spectroscopy at the Mn K-edge, the electronic structure (Mn oxidation states) and coordination geometry of the X-ray-absorbing Mn ions can be studied specifically, without interfering contributions from other redox factors (*39*). Therefore, time-resolved X-ray absorption experiments are ideally suited for monitoring oxidation-state changes of the Mn complex of PSII (*23*, *60*, *61*) and have provided conclusive evidence of an intermediate state, denoted as either as S_4 or S_3^n, attained before ET to Y_Z^{ox} and O_2 formation (*2*, *10*, *12*). These X-ray experiments, however, are exceptionally elaborate and costly because, e.g., collection of one data set at a single pH typically requires the use of several thousand PSII samples and several days of measuring time at a high-performance synchrotron radiation source. For studying the complete pH dependence or sets of PSII mutants, the experimental costs are prohibitive. Therefore, we explored the applicability of near-UV absorption spectroscopy for studying the formation of the intermediate state formed in the course of the $S_3 \rightarrow S_0 + O_2$ transition.

In seminal investigations, several groups have identified the wavelength range around 360 nm to be suitable for monitoring changes in the oxidation state of the Mn complex (*20*, *22*, *40*, *41*, *48*). They found that, apart from a subnanosecond rise that can be assigned to Q_A reduction, acceptor side contributions to the A_{360} signal mostly can be eliminated in the time domain of interest by using suitable artificial electron acceptors. Comparison of the A_{360} transients in Figure 2 and the X-ray absorption transients reported previously (*23*) reveals a high degree of similarity, thereby corroborating that the A_{360} signal is suitable for monitoring the oxidation-state changes of the Mn complex in time-resolved

experiments. However, the stringent correction for contributions by other redox factors (specifically Q_A and Q_B), miss events, and so-called non-Q_B units is mandatory whenever a fully quantitative analysis is approached (Table S1 of the Supporting Information). We note that the excellent quantitative agreement of the near-UV results obtained for PSII membrane particles in solution (in this study) and the X-ray results obtained for partially dehydrated PSII membrane particles (*23*) also confirms that the moderate dehydration in the X-ray experiments remains without influence on the functional characteristics of the donor side reactions in PSII.

The flash-induced oxidation-state changes of the Mn complex have been monitored by time-resolved near-UV difference spectroscopy in the past (*20*−*22*, *40*, *41*, *48*). Mostly a lag-phase behavior in the $S_3 \rightarrow S_0 + O_2$ transition either remained invisible or was not discussed as an indication of formation of a reaction intermediate, yet there are two notable exceptions. In refs *21* and *41*, a lag phase preceding Mn reduction in the $S_3 \rightarrow S_0 + O_2$ transition was detected and interpreted in terms of an intermediate formed by deprotonation (*21*) or in terms of formation of a redox equilibrium involving peroxide bound to the Mn complex (*41*). We feel that investigations of highly active PSII particles, a low noise level, and a stringent deconvolution approach are crucial for determination of the lag-phase duration in the near-UV transients at an adequate level of reliability. The visibility of the delayed onset of O_2 formation in other experiments is discussed elsewhere (*25*).

Formation of an Intermediate by Removal of a Proton from the Mn Complex. Formation of the reaction intermediate in the $S_3 \rightarrow S_0 + O_2$ transition is an essential step in the overall reaction cycle leading to dioxygen formation, but it cannot be assigned to an electron transfer step. It proceeds after oxidation of Y_Z by the P_{680}^+ but before the transfer of an electron from the Mn complex to Y_Z^{ox}, as discussed in refs *23* and *25*. It may involve an essential structural transition or proton relocation. In ref *23*, the formation of the intermediate state is assigned to removal of a proton from the Mn complex, mostly based on analysis of delayed fluorescence (DF) transients (*23*, *36*, *37*) and in line with earlier conclusions of Rappaport and co-workers based on detection of electrochromic absorption changes of PSII pigments (*21*); for a more detailed discussion, see ref *25*.

The process of removal of a proton from the Mn complex to the aqueous phase is not a one-step process but likely involves a chain of donor and acceptor molecules being protonatable residues as well as inner-protein water molecules. The analysis of DF time courses suggests the existence of at least three protonation steps with characteristic rate constants of ~65, ~15, and ~5 ms^{-1} (at pH 6.2) (Figure S8 of ref *23*). The consecutive reaction scheme used here represents an approximation as it invokes only a single rate-determining step, thereby modeling only the slowest proton transfer step. A closer look at the lower curve in Figure 2C indeed reveals a small deviation between the simulated and experimental curve within the first 500 μs: the experimental curve is more sigmoidal than the simulated one, in analogy to the behavior of the X-ray absorption transients in ref *23*. A better agreement is reached assuming the existence of three proton transfer steps (not shown), which has also been observed for the X-ray absorption transients (Figure S8 of ref *23*). However, the numerical value of these faster proton transfer steps cannot be determined by curve fitting at a reasonable level of reliability. Therefore, we modeled the A_{360} transients of the $S_3 \rightarrow S_0 + O_2$ transition by assuming the existence of a single step of proton transfer before electron transfer and O_2 formation, thereby focusing on the slowest, rate-determining event in the sequence of proton transfer steps. We find that this step is significantly slowed in deuterated water and at low pH, in clear contrast to the investigated ET steps (Table 1).

Proton transfer involves the tunneling of a proton from a donor to an acceptor group. The tunneling probability depends on the mass of the tunneling nucleus and is predicted to be strongly reduced for the deuteron (^2H, 2 amu) in comparison to the lighter proton (^1H, 1 amu). Therefore, the existence of a sizable KIE of the lag phase ($k_H/k_D > 2$) strongly supports assignment to a proton transfer step. The KIE depends not only on the tunneling probability but also on the frequency or rate of nuclear movements required for reaching a donor−acceptor distance sufficiently short for proton tunneling (*62*, *63*). Therefore, the magnitude of the KIE is not easily understood in quantitative terms.

The large KIE of the lag-phase reaction could explain why previously obtained KIE values for the slow decay component were larger [k_H/k_D = 1.3 (*64*), 1.4 (*41*), and 1.6 (*22*)] than those found in our present investigation (k_H/k_D = 1.17). Monoexponential simulation of the biphasic time course (lag phase plus millisecond decay) could have resulted in a time-constant value for the millisecond phase that was affected (increased) by the lag-phase duration. An extension of the lag-phase duration upon replacement of H_2O with D_2O thus could explain that for a monoexponential simulation of the absoption transients, higher KIE values have been presented in previous investigations.

We note that the observed lag phase in the $S_3 \rightarrow S_0 + O_2$ transition likely is related to the slower components (up to 100 μs) of the multiphasic P_{680}^+ reduction by Y_Z (*18*, *19*). The microsecond components of the reduction kinetics were sensitive to H−D exchange and have been assigned to relaxation of the Y_Z^{ox} environment accompanied by the rearrangement of H-bond networks. The analysis of the delayed Chl fluorescence suggests that the relocation of the proton from the Mn complex to the aqueous phase is a multistep process (*23*, *37*), and the faster steps may explain the previously observed Y_Z^{ox} relaxation in the early microsecond domain (*18*, *19*) as a stabilization of a positively charged Y_Z^{ox} by relocation of a proton.

Herein we report that at an increased proton concentration (low pH) in the aqueous bulk phase, the putative proton transfer step is decelerated clearly more strongly than any of the ET steps in the S-state cycle (Table 1). The direction and magnitude of the pH effect do not surprise and appear to support, at least qualitatively, formation of the intermediate state by proton transfer and release to the aqueous phase. Three hypothetical mechanisms for deceleration of proton release are discussed here.

(1) In the proton transfer from a peripheral buffer-accessible group of the protein to the aqueous phase, the rate for collision-controlled transfer to hydroxides, which are present at extremely low concentrations only (100 nM at pH 7), is much smaller than for the transfer to mobile buffer molecules that are present at millimolar concentrations [≥25 mM (see Materials and Methods)]. The direct transfer to an H_2O molecule, however, is energetically extremely unfavorable, because of the low proton affinity of a water molecule (p*K* of around −1.7), and therefore is predicted to be slower than the transfer to a mobile buffer present at a millimolar concentration.

Thus, the deprotonation of a peripheral group likely is controlled by collision with a mobile proton acceptor group.

The corresponding rate constant is estimated to be

$$k_H = k_{coll}[\text{mobile proton acceptor}] \quad (2)$$

with a k_{coll} of $\sim 10^8$ M^{-1} s^{-1} (*33*). Taking into account the concentrations of the unprotonated buffer molecules, we predict the time constant of protonation (that is $1/k_H$) to be smaller than 2.5 μs and thus roughly 2 orders of magnitude smaller than the experimentally determined values of τ_{lag}. These quantitative considerations disfavor the possibility that the transfer of a proton from a peripheral base to the aqueous buffer represents the rate-determining step.

(2) A group that is part of the proton transfer path and equilibrates sufficiently fast with the aqueous proton concentration could explain deceleration at low pH if its pK was within the investigated range of pH values. Proton transfer toward this group is "gated" by its protonation state so that the rate constant of transfer may hold (Henderson−Hasselbach equation):

$$k_H = [10^{pH-pK}/(1+10^{pH-pK})]{k_H}^0 \quad (3)$$

where ${k_H}^0$ describes the maximal rate for proton transfer at high pH. Equation 3 cannot provide a fully quantitative description of our experimental findings because it predicts at increasingly low pH values a decrease in k_H (or ${\tau_{lag}}^{-1}$) by a factor of 10 per pH unit, in contrast to the experimental results (τ_{lag} in Figure 6). However, eq 3 relates to a single protonatable group, neglecting pK shifts due to interactions with other ionizable groups. The involvement of a cluster of interacting charged groups could result in strong deviations from eq 3 (*65*, *66*). Moreover, two or more parallel proton transfer paths, possibly even in the form of transfer through a "proton sponge", also might explain the relatively mild deceleration.

(3) The rate constant for proton transfer typically depends on the difference between the pK values of the acceptor group (pK_{accept}) and the donor group (pK_{donor}) (*63*, *67*). If a group close to the proton acceptor were protonated at low pH, then electrostatic interactions could decrease pK_{accept} more than pK_{donor}, thereby diminishing the rate constant of proton transfer significantly. This indirect influence on the rate-determining proton transfer step might provide an explanation for the experimentally determined pH dependence of τ_{lag}.

Option 2 or 3 could explain the pH dependence of the rate-determining step in the formation of the intermediate state in the $S_3 \rightarrow S_0 + O_2$ transition. An in-depth understanding at the atomic level is desirable but will require clearly more extensive investigations involving time-resolved experiments with "proton-sensitive" methods, e.g., infrared spectroscopy (*68*), employment of site mutants, and computational approaches (*66*). The results presented here provide important support for the formation of an additional reaction intermediate in the $S_3 \rightarrow S_0 + O_2$ transition by deprotonation and proton release, as proposed in ref *23*. The putative sequence of events, the role for mechanism, and the energetics of photosynthetic water oxidation are discussed elsewhere in detail (*1*, *25*, *35*, *69*, *70*) and summarized in the following.

Within < 1 μs of the absorption of a photon, Y_Z (Tyr_{161} of the D1 protein) is largely oxidized by ET to ${P_{680}}^+$ (Figure 1B). This ET is coupled to the shift of the phenolic proton from the tyrosine residue to a hydrogen-bonded histidine (His_{190} of the D1 protein), rendering ${Y_Z}^{ox}$ formally a neutral radical. Most likely, the phenolic proton is never released to the lumenal bulk phase but shifts back to the tyrosine side chain upon ${Y_Z}^{ox}$ reduction by the Mn complex [rocking hydrogen bond (*71*)]. Consequently, Y_Z oxidation results in the formation of a positive charge close to ${Y_Z}^{ox}$. The positively charged ${Y_Z}^{ox}$ causes pK shifts of nearby and more distant titratable groups, either by electrostatic through-space interactions or by through-bond interactions originating from modification of the hydrogen bonding network in the vicinity of ${Y_Z}^{ox}$. These pK shifts eventually result in deprotonation of the Mn complex (or its immediate environment). Deprotonation and relocation of protons to the aqueous phase are completed within ~ 200 μs (τ_{lag}), as strongly supported by the results reported here. There are two consequences of the deprotonation for the mechanism of dioxygen formation. First, the deprotonation lowers the redox potential of the Mn complex, thereby facilitating the ET from the Mn complex to ${Y_Z}^{ox}$ (τ_{O_2} of ~ 1.5 ms). Second, either a "substrate water" is directly deprotonated, or a catalytic base that can accept a proton in the ET step to ${Y_Z}^{ox}$ or in the O−O bond formation step is created. The putative base is still unknown. A plausible hypothesis has been put forward by Brudvig and McEvoy (*2*, *70*). On the basis of the crystallographic model of Barber and co-workers (*4*), they proposed that Arg357 of the CP43 subunit is deprotonated in the oxygen evolution transition, as later supported by computational chemistry (*72*).

The sequence of events described above has been proposed on the basis of experimental and theoretical findings of several research groups, as reviewed elsewhere (*1*, *25*, *35*). Many aspects are still (too) hypothetical. The results reported here provide strong evidence that the rate-determining step in formation of the reaction intermediate that has been denoted as S_4 (*23*) or ${S_3}^n$ (*1*) is a proton transfer step. In the future, time-resolved detection of near-UV transients in combination with residue editing by site-directed mutagenesis could facilitate identification of key groups and provide insights into the outlined events at an atomic level.

ACKNOWLEDGMENT

We thank Dr. M. Haumann for valuable discussion and M. Fünning for skillful preparation of PSII membrane particles.

SUPPORTING INFORMATION AVAILABLE

Rationale of the deconvolution procedure and the equations used, steps involved in evaluation of the raw absorption transients described and illustrated (Figure S1), time constants of the lag phase for various deconvolution parameters (Table S1), and pH dependence of the miss parameter (Figure S2). This material is available free of charge via the Internet at http://pubs.acs.org.

REFERENCES

1. Dau, H., and Haumann, M. (2008) The manganese complex of photosystem II in its reaction cycle: Basic framework and possible realization at the atomic level. *Coord. Chem. Rev. 252*, 273–295.
2. McEvoy, J. P., and Brudvig, G. W. (2006) Water-splitting chemistry of photosystem II. *Chem. Rev. 106*, 4455–4483.
3. Debus, R. J. (1992) The manganese and calcium ions of photosynthetic oxygen evolution. *Biochim. Biophys. Acta 1102*, 269–352.
4. Ferreira, K. N., Iverson, T. M., Maghlaoui, K., Barber, J., and Iwata, S. (2004) Architecture of the photosynthetic oxygen-evolving center. *Science 303*, 1831–1838.
5. Guskov, A., Kern, J., Gabdulkhakov, A., Broser, M., Zouni, A., and Saenger, W. (2009) Cyanobacterial photosystem II at 2.9-Å resolution and the role of quinones, lipids, channels and chloride. *Nat. Struct. Mol. Biol. 16*, 334–342.
6. Kamiya, N., and Shen, J.-R. (2003) Crystal structure of oxygen-evolving photosystem II from *Thermosynechococcus vulcanus* at 3.7-Å resolution. *Proc. Natl. Acad. Sci. U.S.A. 100*, 98–103.

7. Dau, H., and Zaharieva, I. (2009) Principles, efficiency, and blueprint character of solar-energy conversion in photosynthetic water oxidation. *Acc. Chem. Res. 42*, 1861–1870.
8. Rappaport, F., and Diner, B. A. (2008) Primary photochemistry and energetics leading to the oxidation of the $(Mn)_4Ca$ cluster and to the evolution of molecular oxygen in Photosystem II. *Coord. Chem. Rev. 252*, 259–272.
9. Dau, H., Limberg, C., Reier, T., Risch, M., Roggan, S., and Strasser, P. (2010) The mechanism of water oxidation: From electrolysis via homogeneous to biological catalysis. *ChemCatChem 2*, 724–761.
10. Cukier, R. I., and Nocera, D. G. (1998) Proton-coupled electron transfer. *Annu. Rev. Phys. Chem. 49*, 337–369.
11. Dau, H., Iuzzolino, L., and Dittmer, J. (2001) The tetra-manganese complex of photosystem II during its redox cycle: X-ray absorption results and mechanistic implications. *Biochim. Biophys. Acta 1503*, 24–39.
12. Junge, W., Haumann, M., Ahlbrink, R., Mulkidjanian, A., and Clausen, J. (2002) Electrostatics and proton transfer in photosynthetic water oxidation. *Philos. Trans. R. Soc. London, Ser. B 357*, 1407–1418.
13. Huynh, M. H. V., and Meyer, T. J. (2007) Proton-coupled electron transfer. *Chem. Rev. 107*, 5004–5064.
14. Hammes-Schiffer, S. (2009) Theory of proton-coupled electron transfer in energy conversion processes. *Acc. Chem. Res. 42*, 1881–1889.
15. Groot, M. L., Pawlowicz, N. P., van Wilderen, L. J. G. W., Breton, J., van Stokkum, I. H. M., and van Grondelle, R. (2005) Initial electron donor and acceptor in isolated Photosystem II reaction centers identified with femtosecond mid-IR spectroscopy. *Proc. Natl. Acad. Sci. U.S.A. 102*, 13087–13092.
16. Holzwarth, A. R., Muller, M. G., Reus, M., Nowaczyk, M., Sander, J., and Rögner, M. (2006) Kinetics and mechanism of electron transfer in intact photosystem II and in the isolated reaction center: Pheophytin is the primary electron acceptor. *Proc. Natl. Acad. Sci. U.S.A. 103*, 6895–6900.
17. Diner, B. A., Schlodder, E., Nixon, P. J., Coleman, W. J., Rappaport, F., Lavergne, J., Vermaas, W. F., and Chisholm, D. A. (2001) Site-directed mutations at D1-His198 and D2-His197 of photosystem II in *Synechocystis* PCC 6803: Sites of primary charge separation and cation and triplet stabilization. *Biochemistry 40*, 9265–9281.
18. Christen, G., and Renger, G. (1999) The role of hydrogen bonds for the multiphasic $P680^{+\bullet}$ reduction by Y_Z in photosystem II with intact oxyen evolution capacity. Analysis of kinetic H/D isotope exchange effects. *Biochemistry 38*, 2068–2077.
19. Schilstra, M. J., Rappaport, F., Nugent, J. H. A., Barnett, C. J., and Klug, D. R. (1998) Proton/hydrogen transfer affects the S-state-dependent microsecond phases of $P680^+$ reduction during water splitting. *Biochemistry 37*, 3974–3981.
20. Dekker, J. P., Plijter, J. J., Ouwehand, L., and van Gorkom, H. J. (1984) Kinetics of manganese redox transitions in the oxygen evolving apparatus of photosynthesis. *Biochim. Biophys. Acta 767*, 176–179.
21. Rappaport, F., Blanchard-Desce, M., and Lavergne, J. (1994) Kinetics of electron transfer and electrochromic change during the redox transition of the photosynthetic oxygen-evolving complex. *Biochim. Biophys. Acta 1184*, 178–192.
22. Karge, M., Irrgang, K. D., and Renger, G. (1997) Analysis of the reaction coordinate of photosynthetic water oxidation by kinetic measurements of 355 nm absorption changes at different temperatures in photosystem II preparations suspended in either H_2O or D_2O. *Biochemistry 36*, 8904–8913.
23. Haumann, M., Liebisch, P., Muller, C., Barra, M., Grabolle, M., and Dau, H. (2005) Photosynthetic O_2 formation tracked by time-resolved X-ray experiments. *Science 310*, 1019–1021.
24. Kok, B., Forbush, B., and McGloin, M. (1970) Cooperation of charges in photosynthetic O_2 evolution. I. A linear four-step mechanism. *Photochem. Photobiol. 11*, 457–475.
25. Dau, H., and Haumann, M. (2007) Time-resolved X-ray spectroscopy leads to an extension of the classical S-state cycle model of photosynthetic oxygen evolution. *Photosynth. Res. 92*, 327–343.
26. Haumann, M., Muller, C., Liebisch, P., Iuzzolino, L., Dittmer, J., Grabolle, M., Neisius, T., Meyer-Klaucke, W., and Dau, H. (2005) Structural and oxidation state changes of the photosystem II manganese complex in four transitions of the water oxidation cycle ($S_0 \rightarrow S_1$, $S_1 \rightarrow S_2$, $S_2 \rightarrow S_3$, and $S_{3,4} \rightarrow S_0$) characterized by X-ray absorption spectroscopy at 20 K and room temperature. *Biochemistry 44*, 1894–1908.
27. Messinger, J., Robblee, J. H., Bergmann, U., Fernandez, C., Glatzel, P., Visser, H., Cinco, R. M., McFarlane, K. L., Bellacchio, E., Pizarro, S. A., Cramer, S. P., Sauer, K., Klein, M. P., and Yachandra, V. K. (2001) Absence of Mn-centered oxidation in the $S_2 \rightarrow S_3$ transition: Implications for the mechanism of photosynthetic water oxidation. *J. Am. Chem. Soc. 123*, 7804–7820.
28. Kuzek, D., and Pace, R. J. (2001) Probing Mn oxidation states in the OEC. Insights from spectroscopic, computational and kinetic data. *Biochim. Biophys. Acta 1503*, 123–137.
29. Carrell, G., Tyryshkin, M., and Dismukes, C. (2002) An evaluation of structural models for the photosynthetic water-oxidizing complex derived from spectroscopic and X-ray diffraction signatures. *J. Biol. Inorg. Chem. 7*, 2–22.
30. Robblee, J. H., Cinco, R. M., and Yachandra, V. K. (2001) X-ray spectroscopy-based structure of the Mn cluster and mechanism of photosynthetic oxygen evolution. *Biochim. Biophys. Acta 1503*, 7–23.
31. Jahns, P., Lavergne, J., Rappaport, F., and Junge, W. (1991) Stoichiometry of Proton Release During Photosynthetic Water Oxidation: A Reinterpretation of the Responses of Neutral Red Leads to a Non-integer Pattern. *Biochim. Biophys. Acta 1057*, 313–319.
32. Rappaport, F., and Lavergne, J. (1991) Proton release during successive oxidation steps of the photosynthetic water oxidation process: Stoichiometries and pH dependence. *Biochemistry 30*, 10004–10012.
33. Haumann, M., and Junge, W. (1994) Extent and rate of proton release by photosynthetic water oxidation in thylakoids: Electrostatic relaxation versus chemical production. *Biochemistry 33*, 864–872.
34. Schlodder, E., and Witt, H. T. (1999) Stoichiometry of proton release from the catalytic center in photosynthetic water oxidation. Reexamination by a glass electrode study at pH 5.5−7.2. *J. Biol. Chem. 274*, 30387–30392.
35. Dau, H., and Haumann, M. (2007) Eight steps preceding O-O bond formation in oxygenic photosynthesis: A basic reaction cycle of the Photosystem II manganese complex. *Biochim. Biophys. Acta 1767*, 472–483.
36. Grabolle, M., and Dau, H. (2005) Energetics of primary and secondary electron transfer in Photosystem II membrane particles of spinach revisited on basis of recombination-fluorescence measurements *Biochim. Biophys. Acta 1708*, 209–218.
37. Buchta, J., Grabolle, M., and Dau, H. (2007) Photosynthetic dioxygen formation studied by time-resolved delayed fluorescence measurements: Method, rationale, and results on the activation energy of dioxygen formation. *Biochim. Biophys. Acta 1767*, 565–574.
38. Lavergne, J., and Junge, W. (1993) Proton release during the redox cycle of the water oxidase. *Photosynth. Res. 38*, 279–296.
39. Dau, H., Liebisch, P., and Haumann, M. (2003) X-ray absorption spectroscopy to analyze nuclear geometry and electronic structure of biological metal centers: Potential and questions examined with special focus on the tetra-nuclear manganese complex of oxygenic photosynthesis. *Anal. Bioanal. Chem. 376*, 562–583.
40. Saygin, Ö., and Witt, H. T. (1987) Optical characterization of intermediates in the water-splitting enzyme system of photosynthesis: Possible states and configurations of manganese and water. *Biochim. Biophys. Acta 893*, 452–469.
41. Haumann, M., Bögershausen, O., Cherepanov, D., Ahlbrink, R., and Junge, W. (1997) Photosynthetic oxygen evolution: H/D isotope effects and the coupling between electron and proton transfer during the redox reactions at the oxidizing side of Photosystem II *Photosynth. Res. 51*, 193–208.
42. Renger, G. (2007) Oxidative photosynthetic water splitting: Energetics, kinetics and mechanism. *Photosynth. Res. 92*, 407–425.
43. Berthold, D. A., Babcock, G. T., and Yocum, C. F. (1981) A Highly Resolved, Oxygen-Evolving Photosystem II Preparation from Spinach Thylakoid Membranes: EPR and Electron-Transport Properties. *FEBS Lett. 134*, 231–234.
44. Schiller, H., and Dau, H. (2000) Preparation protocols for high-activity Photosystem II membrane particles of green algae and higher plants, pH dependence of oxygen evolution and comparison of the S_2-state multiline signal by X-band EPR spectroscopy. *J. Photochem. Photobiol., B 55*, 138–144.
45. Lavergne, J. (1991) Improved UV-visible spectra of the S-transitions in the photosynthetic oxygen-evolving system. *Biochim. Biophys. Acta 1060*, 175–188.
46. Schatz, G. H., and van Gorkom, H. J. (1985) Absorbance Difference Spectra Upon Charge-Transfer to Secondary Donors and Acceptors in Photosystem II. *Biochim. Biophys. Acta 810*, 283–294.
47. Renger, G., and Hanssum, B. (1988) Studies on the deconvolution of flash-induced absorption changes into the difference spectra of individual redox steps within the water-oxidizing enzyme system. *Photosynth. Res. 16*, 243–259.
48. Renger, G., and Weiss, W. (1986) Studies on the Nature of the Water-Oxidizing Enzyme. 3. Spectral Characterization of the Intermediary Redox States in the Water-Oxidizing Enzyme System-Y. *Biochim. Biophys. Acta 850*, 184–196.
49. Lavergne, J., and Leci, E. (1993) Properties of Inactive Photosystem II Centers. *Photosynth. Res. 35*, 323–343.

50. Grabolle, M., and Dau, H. (2007) Efficiency and role of loss processes in light-driven water oxidation by PSII. *Physiol. Plant. 131*, 50–63.
51. Thapper, A., Mamedov, F., Mokvist, F., Hammarström, L., and Styring, S. (2009) Defining the Far-Red Limit of Photosystem II in Spinach. *Plant Cell 21*, 2391–2401.
52. Rappaport, F., Guergova-Kuras, M., Nixon, P. J., Diner, B. A., and Lavergne, J. (2002) Kinetics and pathways of charge recombination in Photosystem II. *Biochemistry 41*, 8518–8527.
53. Iuzzolino, L., Dittmer, J., Dörner, W., Meyer-Klaucke, W., and Dau, H. (1998) X-ray absorption spectroscopy on layered photosystem II membrane particles suggests manganese-centered oxidation of the oxygen-evolving complex for the S_0-S_1, S_1-S_2, and S_2-S_3 transitions of the water oxidation cycle. *Biochemistry 37*, 17112–17119.
54. Messinger, J., and Renger, G. (1994) Analyses of pH-induced modifications of the period four oscillation of flash-induced oxygen evolution reveal distinct structural changes of the photosystem II donor side at characteristic pH values. *Biochemistry 33*, 10896–10905.
55. Christen, G., Seeliger, A., and Renger, G. (1999) $P680^{+\bullet}$ Reduction Kinetics and Redox Transition Probability of the Water Oxidizing Complex as a Function of pH and H/D Isotope Exchange in Spinach Thylakoids. *Biochemistry 38*, 6082–6092.
56. Bernát, G., Morvaridi, F., Feyziyev, Y., and Styring, S. (2002) pH-dependence of the four individual transitions in the catalytic S-cycle during photosynthetic oxygen evolution. *Biochemistry 41*, 5830–5843.
57. Suzuki, H., Sugiura, M., and Noguchi, T. (2005) pH dependence of the flash-induced S-state transitions in the oxygen-evolving center of photosystem II from *Thermosynechoccocus elongatus* as revealed by Fourier transform infrared spectroscopy. *Biochemistry 44*, 1708–1718.
58. Krohs, U., and Metzner, H. (1990) Overall kinetics of photosystem-II: pH-dependence and deuterium-isotope effect. *Bioelectrochem. Bioenerg. 23*, 141–152.
59. Lydakis-Simantiris, N., Ghanotakis, D. F., and Babcock, G. T. (1997) Kinetic isotope effects on the reduction of the Y_Z radical in oxygen evolving and tris-washed Photosystem II membranes by time-resolved EPR. *Biochim. Biophys. Acta 1322*, 129–140.
60. Haumann, M., Müller, C., Liebisch, P., Neisius, T., and Dau, H. (2005) A novel BioXAS technique with sub-millisecond time resolution to track oxidation state and structural changes at biological metal centers. *J. Synchrotron Radiat. 12*, 35–44.
61. Haumann, M., Grundmeier, A., Zaharieva, I., and Dau, H. (2008) Photosynthetic water oxidation at elevated dioxygen partial pressure monitored by time-resolved X-ray absorption measurements. *Proc. Natl. Acad. Sci. U.S.A. 105*, 17384–17389.
62. Krishtalik, L. I. (2000) The mechanism of the proton transfer: An outline. *Biochim. Biophys. Acta 1458*, 6–27.
63. Hammes-Schiffer, S. (2006) Hydrogen tunneling and protein motion in enzyme reactions. *Acc. Chem. Res. 39*, 93–100.
64. Renger, G., Bittner, T., and Messinger, J. (1994) Structure-Function Relationships in Photosynthetic Water Oxidation. *Biochem. Soc. Trans. 22*, 318–322.
65. Yang, A. S., Gunner, M. R., Sampogna, R., Sharp, K., and Honig, B. (1993) On the calculation of p*K*as in proteins. *Proteins 15*, 262–265.
66. Ishikita, H., Saenger, W., Loll, B., Biesiadka, J., and Knapp, E. W. (2006) Energetics of a possible proton exit pathway for water oxidation in photosystem II. *Biochemistry 45*, 2063–2071.
67. Marcus, M. A. (1968) Theoretical relations among rate constants, barriers, and Brønsted slopes of chemical reactions. *J. Phys. Chem. 72*, 891–899.
68. Barry, B. A., Cooper, I. B., De Riso, A., Brewer, S. H., Vu, D. M., and Dyer, R. B. (2006) Time-resolved vibrational spectroscopy detects protein-based intermediates in the photosynthetic oxygen-evolving cycle. *Proc. Natl. Acad. Sci. U.S.A. 103*, 7288–7291.
69. Dau, H., and Haumann, M. (2006) Reaction cycle of photosynthetic water oxidation in plants and cyanobacteria (response letter). *Science 312*, 1471–1472.
70. McEvoy, J. P., and Brudvig, G. W. (2004) Structure-based mechanism of photosynthetic water oxidation. *Phys. Chem. Chem. Phys. 6*, 4754–4763.
71. Ahlbrink, R., Haumann, M., Cherepanov, D., Boegershausen, O., Mulkidjanian, A., and Junge, W. (1998) Function of tyrosine-Z in water oxidation by photosystem II: Electrostatical promotor instead of hydrogen abstractor. *Biochemistry 37*, 1131–1142.
72. Sproviero, E. M., Gascon, J. A., McEvoy, J. P., Brudvig, G. W., and Batista, V. S. (2008) Quantum mechanics/molecular mechanics study of the catalytic cycle of water splitting in photosystem II. *J. Am. Chem. Soc. 130*, 3428–3442.